

Pressure-Induced Chemical Decomposition and Structural Changes of Boric Acid

Alexei Yu. Kuznetsov,^{*,†} Altair S. Pereira,[‡] Andrei A. Shiryayev,[§] Julien Haines,^{||} Leonid Dubrovinsky,[†] Vladimir Dmitriev,[⊥] Phil Pattison,[⊥] and Nicolas Guignot[⊥]

Bayerisches Geoinstitut, Universität Bayreuth, D-95440 Bayreuth, Germany, Instituto de Física e Escola de Engenharia, Universidade Federal do Rio Grande do Sul, 91501-970, Porto Alegre, RS, Brazil, Institute of Crystallography RAS, Leninsky Pr. 59, Moscow 119333, Russia, Laboratoire de Physico-Chimie de la Matière Condensée, Université Montpellier II, Montpellier Cedex 5, France, and European Synchrotron Radiation Facility, BP 220, 38043 Grenoble Cedex, France

Received: March 16, 2006; In Final Form: May 18, 2006

A combined synchrotron X-ray diffraction, Raman scattering, and infrared spectroscopy study of the pressure-induced changes in H_3BO_3 to 10 GPa revealed a new high-pressure phase transition between 1 and 2 GPa followed by chemical decomposition into cubic HBO_2 , ice-VI, and ice-VII at ~ 2 GPa. The layered triclinic structure of H_3BO_3 exhibits a highly anisotropic compression with maximum compression along the c direction, accompanied by a strong reduction of the interlayer spacing. The large volume variation and structural changes accompanying the decomposition suggest high activation energy. This yields a slow reaction kinetics at room temperature and a phase composition that is highly dependent on the specific pressure–time path followed by the sample. The combined results have been used to propose a mechanism for pressure-induced dehydration of H_3BO_3 that implies a proton disorder in the system.

Introduction

Boric acid, H_3BO_3 , is one of the first compounds with a hydrogen-bonded crystal structure to be characterized by X-ray diffraction methods.¹ Its triclinic crystal structure, space group $P\bar{1}$, consists of a layered packing of slightly buckled sheets.² Each sheet is formed by H_3BO_3 molecular units with nearly perfect C_{3h} symmetry, linked together by hydrogen bonds $\text{O} \cdots \text{H} \cdots \text{O}$. Ab initio calculations³ show that the binding energy of the sheets is about one-third of the intralayer interaction energy. The relatively low energy needed to promote the mutual sliding between layers of such a structure has been invoked to explain the lubricant properties of boric acid films on the surface of boron-containing materials.⁴ However, lubricant materials can be subjected to compression and heating in applications, and possible changes in the properties of boric acid under such pressure–temperature conditions require an investigation.

The behavior of H_3BO_3 under heating is well-known because of the comprehensive work of Kracek et al.⁵ H_3BO_3 undergoes a dehydration, which starts between 80 and 130 °C depending on the heating rate,⁶ leading to the formation of HBO_2 (metaboric acid), and at higher temperatures, B_2O_3 is produced. Metaboric acid can crystallize in three different forms: γ - HBO_2 (cubic), β - HBO_2 (monoclinic), and α - HBO_2 (orthorhombic). The cubic phase is the most stable and the densest among the crystalline forms of metaboric acid.⁵

In contrast to temperature-induced changes of H_3BO_3 , the influence of pressure on the structure and stability of H_3BO_3 has only recently been addressed. In situ X-ray diffraction

(XRD) studies using conventional X-ray tubes have identified a pressure-induced decomposition (PID) of H_3BO_3 to a mixture of HBO_2 and H_2O .^{7,8} However, some questions remained about the structural changes induced by pressure and the possible formation of new phases of boric acid⁹ at the early stages of PID.

To elucidate the structural aspects of the pressure-induced decomposition of H_3BO_3 and the possible role of hydrogen bonds in the observed transformations, we have performed in situ XRD measurements using a focused beam from a third-generation synchrotron source at high pressures. In this paper, we report the XRD results along with complementary Raman and IR results at high pressures. We will discuss the details of the compression behavior of H_3BO_3 . Our results suggest the role of pressure-induced proton disorder accompanying PID and a new phase transition in H_3BO_3 .

Experimental Procedures

The high-pressure studies of boric acid were carried out on reagent grade H_3BO_3 powder with 99.9% purity in diamond-anvil cells (DAC) without a pressure-transmitting medium. Small crystals of ruby provided a pressure calibration of the sample at room temperature by the standard fluorescence technique.¹⁰ Two structural data sets were obtained at the European Synchrotron Radiation Facility (ESRF, Grenoble, France): one at the ID30 beam line and the other at Swiss Norwegian Beam Lines (BM1A). In-situ high-pressure measurements employed the angle-dispersive X-ray powder diffraction technique with monochromatic ($\lambda = 0.3738$ Å, ID30; $\lambda = 0.71$ Å, BM1A) X-radiation. Diffraction patterns were collected with an image plate detector (MAR345). One-dimensional 2θ dependences of the X-ray diffracted intensities were obtained by integration of two-dimensional diffraction images using the ESRF Fit2D software.¹¹

The Raman scattering measurements were carried out at Bayerisches Geoinstitut using a DILOR XY system with a 5145

* To whom correspondence should be addressed. E-mail: Alexei.Kuznetsov@uni-bayreuth.de.

[†] Bayerisches Geoinstitut.

[‡] Instituto de Física e Escola de Engenharia.

[§] Institute of Crystallography.

^{||} Laboratoire de Physico-Chimie de la Matière Condensée.

[⊥] European Synchrotron Radiation Facility.

Å Ar-ion laser as the excitation source. The incident laser power varied in the range 150–180 mW. The spectrometer was calibrated using the Si Γ_{25} phonon prior to each measurement. Raman spectra were collected in the 100–4000 cm^{-1} range. The high-pressure IR measurements followed the Raman data collection at each pressure step. The IR spectra were obtained in reflection mode using a BrukerIFS 120 high-resolution FTIR spectrometer with a Bruker IR microscope. A thin platinum foil was placed in the gasket hole of the DAC assemblage and was covered by the sample, thus providing a reflection surface for the incident IR radiation. Therefore, each IR spectrum consists of strong transmission and minor reflection components. The sum of 500 scans at 4 cm^{-1} resolution in the range 600–4000 cm^{-1} defined each high-pressure IR spectrum.

Results

(1) X-ray Diffraction. The known triclinic structure of boric acid² described perfectly the powder diffraction patterns collected from the starting H_3BO_3 sample at ambient conditions. However, the relative intensities of the diffraction peaks suffered a significant alteration at ambient pressure just after a compaction of the sample (Figure 1). We attribute this alteration to a preferred orientation of crystallites, which develops at slight non-hydrostatic squeezing of the sample. Subsequent compression to about 2 GPa results in a continuous variation of the diffraction spectra (Figure 2). Despite preferred orientation effects that precluded a full structural refinement, a Le Bail fit provided an excellent description of the observed diffraction patterns in terms of the known triclinic phase of H_3BO_3 . At the same time, some discrepancies between theoretical and experimental diffraction patterns could be observed at pressures above 1 GPa. A new peak, which appeared at 2θ near 4.2 degrees (indicated by an arrow in Figure 2) and a visible misfit in calculated and experimental intensities at low 2θ values indicate some structural changes and a new phase of H_3BO_3 .

The overall close agreement between the XRD patterns of the ambient triclinic phase and that of the new phase suggests that the two are closely related structures. We considered as a possible candidate for the new phase of H_3BO_3 , a new stacking sequence of sheets of hydrogen bonded $\text{B}(\text{OH})_3$ molecules. Figure 3a,b compares the theoretical and experimental diffraction patterns of the boric acid with 2 and 3 sheets per translational period c , respectively. The three-layered structure accounts for the new peak and gives better reliability indices of the profile fit ($R_{\text{wp}} = 0.011$) than the two-layered structure ($R_{\text{wp}} = 0.038$). This result provides evidence that in compressed H_3BO_3 , the way of stacking of sheets may not be longer, the same as at ambient conditions. It is useful to note that a three-layered periodicity has been already reported for a new trigonal polytype of the boric acid.⁹

The increase of pressure to about 2 GPa results in a fast decrease of the parameter c of the triclinic lattice of H_3BO_3 compared with the respective changes of a and b lattice parameters (Figure 4). Such behavior of the lattice parameters fits well with the theoretical predictions³ from which one can expect a higher compressibility of the H_3BO_3 structure along the crystallographic axis c than along the a or b axis. A useful diagnostic procedure can be applied to pressure–volume measurements to check the presence of the phase transition in H_3BO_3 .¹² Figure 5 shows the plot of Birch's¹³ normalized stress $F = P \cdot [3f(1+2f)^{5/2}]^{-1}$ against Eulerian strain $f = 0.5 \cdot [(V_0/V)^{2/3} - 1]$. Two distinct sets of data points with nearly linear behavior as a function of f indicate a change in compressibility of H_3BO_3 , starting from about 1 GPa, and, consequently, a phase

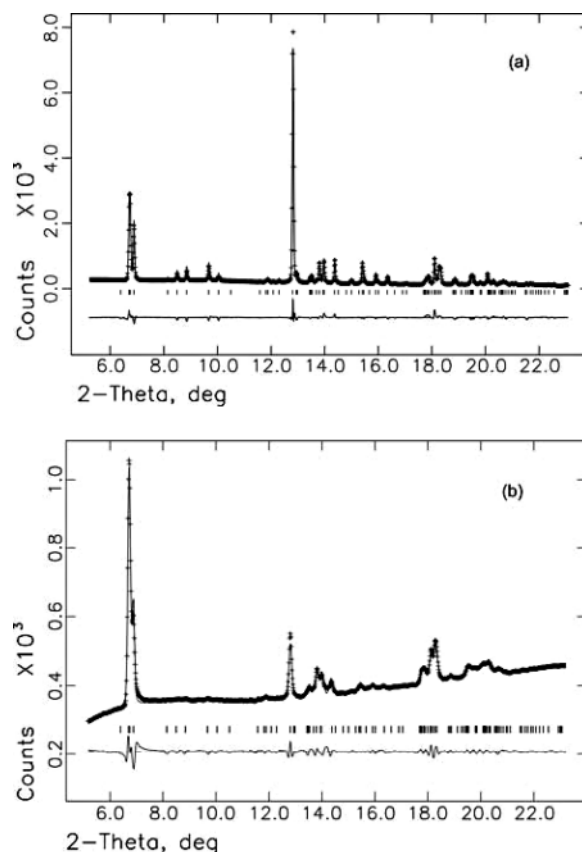


Figure 1. Experimental (crosses) X-ray powder diffraction patterns for H_3BO_3 samples (a) in a rotating capillary and (b) in a diamond anvil cell. The data were recorded at room temperature and ambient pressure with the X-ray wavelength 0.71 Å. Theoretical (solid lines) spectra represent (a) the Rietveld ($R_p = 0.046$ and $R_{\text{wp}} = 0.069$) and (b) Le Bail fit ($R_p = 0.007$ and $R_{\text{wp}} = 0.013$) of the structural model of H_3BO_3 using GSAS program. Hydrogen atoms were not considered in the Rietveld refinement of H_3BO_3 structure (space group $P\bar{1}$) that yielded the following lattice parameters: $a = 7.0296(3)$, $b = 7.0440(3)$, $c = 6.5721(1)$, $\alpha = 92.583(4)$, $\beta = 101.142(4)$, $\gamma = 119.799(2)$. The BO_3 molecular complexes are constrained to C_{3h} symmetry with the refined boron–oxygen distances equal to 1.384 Å. The x , y , and z fractional atomic coordinates for the two boron and six oxygen atoms in the asymmetric unit are: $\text{B}_{(1)} = 0.6492, 0.4204, 0.2511$; $\text{B}_{(2)} = 0.3016, 0.7512, 0.2418$; $\text{O}_{(1)} = 0.7754, 0.3198, 0.2496$; $\text{O}_{(2)} = 0.7491, 0.6465, 0.2515$; $\text{O}_{(3)} = 0.4231, 0.295, 0.2523$; $\text{O}_{(4)} = 0.5289, 0.873, 0.2442$; $\text{O}_{(5)} = 0.1782, 0.8552, 0.2373$; $\text{O}_{(6)} = 0.1978, 0.5253, 0.2439$.

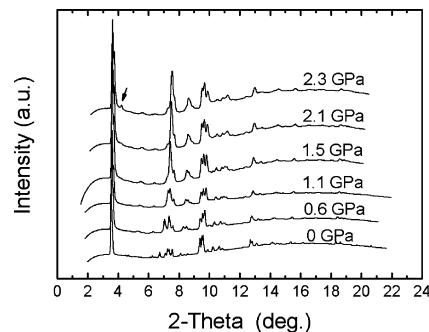


Figure 2. Evolution of the X-ray diffraction patterns of H_3BO_3 with increasing pressure. The spectra were recorded with X-radiation of wavelength 0.3738 Å. The arrow indicates a peak that cannot be accounted for by triclinic lattice of the boric acid (see details in the text).

transition. The intercept of the line that represents the behavior of the data points with $F(f)$ at $f = 0$ yields the bulk modulus B_0 . One can see that B_0 is higher in the low-pressure phase

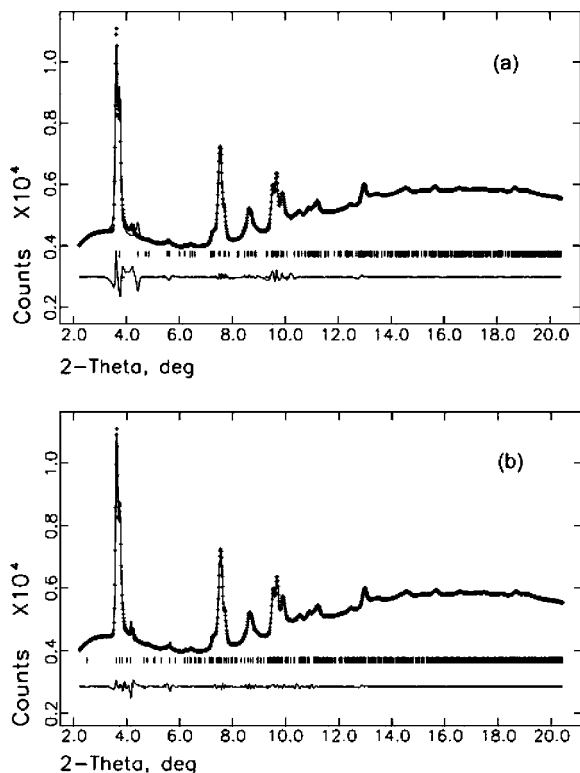


Figure 3. Experimental (crosses) diffraction pattern of H_3BO_3 at 2.3 GPa and ambient temperature ($\lambda = 0.3738 \text{ \AA}$). Solid lines represent the calculated (GSAS, Le Bail fit) diffraction spectra for (a) the structural model with a triclinic lattice which assumes 2 layers of hydrogen bonded $\text{B}(\text{OH})_3$ molecules per translational period along the c axis and (b) 3-layered structural model of the boric acid.

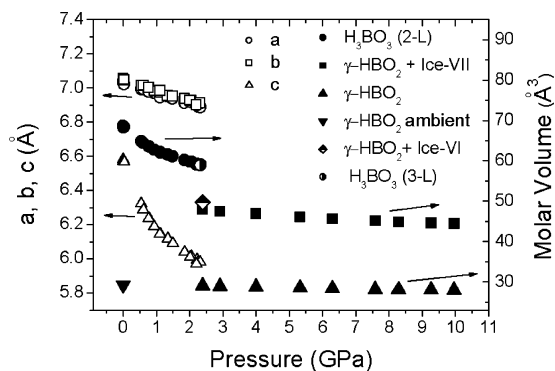


Figure 4. Pressure-induced variation of the lattice parameters and molar volume of H_3BO_3 , and the decomposition products HBO_2 and ice. Open circles, squares, and triangles are the a , b , c lattice parameters of triclinic H_3BO_3 , respectively. Solid circles and triangles are, respectively, the molar volumes of triclinic H_3BO_3 and cubic HBO_2 . Solid squares and half-solid diamond refer to the sum of the molecular volumes of HBO_2 and ice-VII phases and to the sum of HBO_2 and ice-VI molar volumes, respectively. The inverted solid triangle at ambient pressure represents the molar volume of cubic HBO_2 phase.²⁷ The half-solid circle at 2.3 GPa shows the molar volume of a 3-layered structure of H_3BO_3 .

than in the high-pressure phase of H_3BO_3 . On the other hand, the pressure derivative of the bulk modulus B' , which is characterized by the line's slope, is essentially higher for the high-pressure polymorph of boric acid. This relationship between bulk moduli and pressure derivatives of the low- and high-pressure polymorphs can be attributed to the onset of new, stronger interactions in the high-pressure phase of H_3BO_3 that result in a fast decrease of its compressibility.

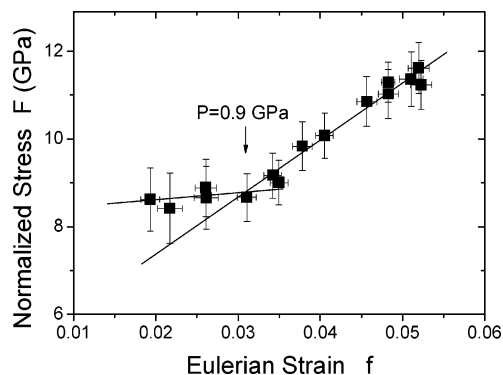


Figure 5. Birch's normalized stress F as a function of the Eulerian strain f . The lines are the guides for eyes.

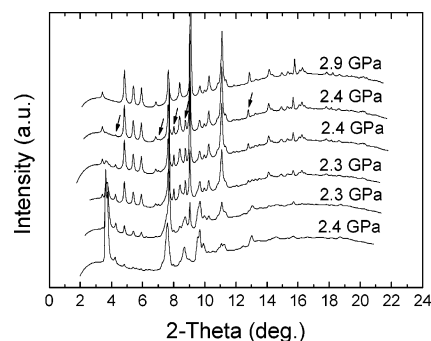


Figure 6. Evolution of the X-ray diffraction patterns of H_3BO_3 during the chemical decomposition process at average pressure about 2.3 GPa ($\lambda = 0.3738 \text{ \AA}$). Some peaks originating from ice-VI (at 2-theta around 7° , 8.2° and 9°) and ice-VII (at 2-theta around 13°) nonoverlapping with the peaks from cubic HBO_2 are indicated by arrows. The peak at about 4.2° corresponds to the new peak of H_3BO_3 indicated in Figure 2. Peaks from ice-VI phase disappear on further compression to 2.9 GPa.

New reflections originating from the decomposition products of H_3BO_3 are clearly seen in the XRD patterns recorded at pressures above 2 GPa (Figure 6). Three new phases were identified at 2.3 GPa: cubic metaboric acid ($\gamma\text{-HBO}_2$, $a = 8.8693(3) \text{ \AA}$), tetragonal ice-VI ($a = 6.0871(8) \text{ \AA}$, $b = 5.579(2) \text{ \AA}$) and cubic ice-VII ($a = 3.3552(7) \text{ \AA}$), thus confirming the pressure-induced decomposition of H_3BO_3 to HBO_2 and H_2O at ambient temperature. The presence of two phases of ice can be attributed to the pressure nonhomogeneity during the decomposition process. Figure 6 shows the selected angle-resolved X-ray diffraction patterns of the sample, covering the decomposition process. The formation of decomposition products was accompanied by a drop of the pressure in the pressure chamber. We compensated this pressure drop by a slight increase of the pressure after each data collection. The pressure was kept within the 2.1–2.7 GPa range during the chemical decomposition, which took about 2 h. The decomposition products, $\gamma\text{-HBO}_2$, ice-VI, and ice-VII, perfectly accounted for all features in the final diffraction pattern at about 2.4 GPa (Figure 7). Subsequent pressure increase to about 3 GPa resulted in a two-phase mixture of $\gamma\text{-HBO}_2$ and ice-VII, which was observed up to 10 GPa, the highest pressure of the diffraction experiments. Figure 4 summarizes the variation of volumes of all observed phases. One can see that the chemical decomposition of H_3BO_3 to HBO_2 and H_2O results in a large overall volume reduction, suggesting a high driving force for this pressure-induced reaction.

(2) Raman and IR Spectroscopy. Raman and IR spectra (Figure 8 and Figure 9) obtained at ambient conditions

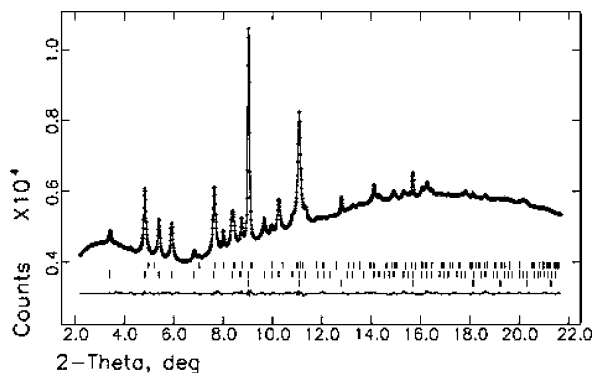


Figure 7. Experimental diffraction pattern at the end of the chemical decomposition of H_3BO_3 at 2.4 GPa (crosses) and Rietveld fit (GSAS, solid line) of $\gamma\text{-HBO}_2$, ice-VI, and ice-VII structures. Upper, middle, and lower tick marks indicate the positions of the Bragg reflections of ice-VI, $\gamma\text{-HBO}_2$, and ice-VII, respectively.

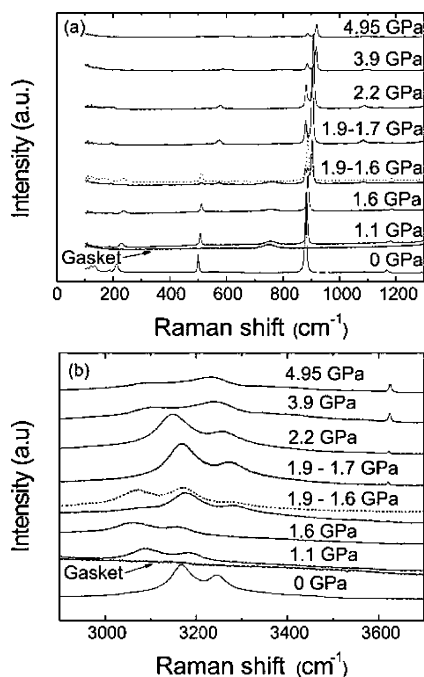


Figure 8. Pressure evolution of the Raman spectra of H_3BO_3 across the decomposition into HBO_2 and H_2O (a) in the frequency range 100–1300 cm^{-1} and (b) from 2900 to 3700 cm^{-1} (higher magnification scale for peaks intensities). The Raman spectrum of the gasket at 1.1 GPa is shown for comparison. Solid and dotted lines at 1.6 GPa represent two spectra taken from different places of the sample, which was initially compressed to 1.9 GPa and kept for 14 h in a DAC.

demonstrated a good agreement with the Raman and IR spectra of the boric acid reported in earlier studies.^{6,14–18} A thorough analysis of the vibrational behavior of boric acid at ambient pressure with an overview of the previous studies was given by Durig et al.¹⁷ Durig et al. showed that the description of H_3BO_3 , which is based on the ideal C_{3h} symmetry of the boric acid molecules and a layer unit cell which contains two such molecules, is the only one that reconciles the IR and Raman data for the intramolecular motions. This “layer-unit-cell” approach was proposed by Bethell and Sheppard,¹⁴ who also gave an ample summary of the earliest Raman and IR spectroscopy studies of H_3BO_3 . The Raman and IR bands of the present study were assigned according to the interpretations of the respective spectra given by Durig et al.¹⁷

The strong bands in the ambient-pressure Raman spectrum of Figure 8a at 500, 880, and 1167 cm^{-1} are the $\nu_{13}(\text{E}_{2g})$ in-

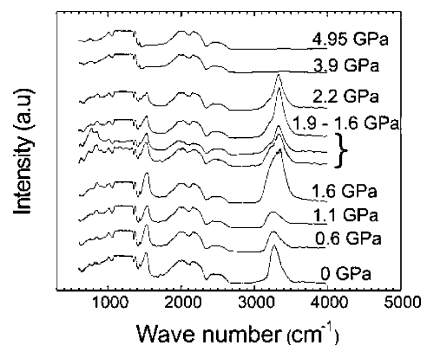


Figure 9. Pressure evolution of FTIR spectra of H_3BO_3 across the chemical decomposition on HBO_2 and H_2O .

plane O–B–O angle deformation, $\nu_{12}(\text{A}_g)$ symmetric B–O bond stretching, and $\nu_{10}(\text{E}_{2g})$ in-plane B–O–H angle deformation modes, respectively. The Raman bands observed at 3168 and 3245 cm^{-1} (Figure 8b, ambient pressure spectrum) correspond to the two Raman active $\nu_8(\text{A}_g)$ symmetric and $\nu_7(\text{E}_{2g})$ antisymmetric O–H bond stretching vibrations, respectively. The bands observed at ambient conditions below 400 cm^{-1} can be assigned to the lattice modes. In particular, the peaks at 187 and 212 cm^{-1} correspond to the symmetric librations in the tentative assignment by Durig et al.

IR spectra of the sample were dominated by the features coming from nitrogen defects and diamond lattice in the ranges from 900 to 1400 cm^{-1} and from 1800 to 2700 cm^{-1} , respectively (Figure 9). Because diamond absorption does not change noticeably within the studied pressure range, its contribution to the IR spectra can be easily distinguished from that of the sample. Several infrared bands originating from the sample could be identified in the regions of spectra free of diamond bands. In the ambient pressure spectrum, two strong bands at about 1520 and 3275 cm^{-1} can be assigned to the two infrared active fundamentals of boric acid: $\nu_2(\text{E}_{1u})$ B–O bond stretching mode and $\nu_1(\text{E}_{1u})$ O–H bond stretching vibration (though our values are higher than reported in the literature). The weak band at about 840 cm^{-1} can be interpreted either as $\nu_4(\text{A}_u)$ out-of-plane O–H deformation mode according to Durig et al.¹⁷ or as $\nu_5(\text{A}_u)$ out-of-plane BO_3 angle deformation mode according to Bethell and Sheppard.¹⁴ The detailed discussion of the pressure behavior of this band and the possible choice between the latter two assignments will be given below.

On compression of the sample, several pressure intervals could be distinguished on the basis of the observed changes in the Raman and IR spectra. The pressure increase from the ambient to 1.6 GPa produces a continuous shift of the Raman and IR peaks described above in the respective spectra. Raman active $\nu_{13}(\text{E}_{2g})$, $\nu_{12}(\text{A}_g)$, and $\nu_{10}(\text{E}_{2g})$ modes shift toward higher frequencies with a nearly linear pressure dependence. We obtained the pressure coefficient of 4.5 $\text{cm}^{-1}/\text{GPa}$ for the frequency shift of $\nu_{12}(\text{E}_{2g})$ symmetric B–O stretching mode. This value is close to that of $\text{B}(\text{OH})_3$ in aqueous fluids observed by Schmidt et al.¹⁹ The $\nu_{13}(\text{A}_g)$ O–B–O bending and the $\nu_{10}(\text{E}_{2g})$ in plane B–O–H bending vibrations exhibit pressure coefficients of 7 and 10.9 $\text{cm}^{-1}/\text{GPa}$, respectively. The difference between the latter values may reflect a higher strengthening on compression of hydrogen bonds in comparison with B–O bonds, as well as some changes in molecular geometry. These changes in molecular geometry are also reflected in the IR spectra: in the O–H stretching region, a new band, corresponding to weaker hydrogen bonds, appears and the band at 1530 cm^{-1} progressively becomes broader, suggesting a poorly resolved doublet. Different behavior is also exhibited by the

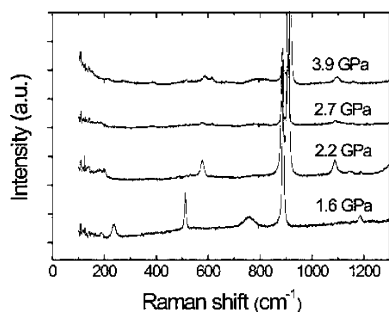


Figure 10. Selected Raman spectra of H_3BO_3 showing the details of the pressure-induced changes across the chemical decomposition into HBO_2 and H_2O in the frequency range 100–1300 cm^{-1} .

bands at 187 and 211 cm^{-1} ascribed to librations of boric acid molecules in the Raman spectra: whereas the former is almost fixed (1.8 $\text{cm}^{-1}/\text{GPa}$), the latter shows the strong pressure shift of 15.3 $\text{cm}^{-1}/\text{GPa}$. The above changes in the pressure range 0–1.6 GPa are consistent with the progressive appearance of a new phase with weaker H bonds and slightly different symmetry of $\text{B}(\text{OH})_3$ molecules.

Drastic changes in Raman and considerable changes in IR spectra associated with the chemical decomposition of H_3BO_3 were observed at pressures above 1.6 GPa. The pressure of the sample varied during the decomposition process as with the X-ray diffraction experiments and was kept for about 15 h within the 1.6–1.9 GPa range during successive data collections. We attribute this pressure variation to the volume changes accompanying the decomposition of H_3BO_3 (see Figure 4) when the sample pressure is increased above some critical value. This negative feedback on the pressure increase during PID allowed for establishing the critical pressure of decomposition equal to 1.6 GPa. It corresponds to the minimal pressure reached by the sample, which consists of the initial H_3BO_3 and its decomposition products, after sufficiently long time without additional external compression. In contrast to the synchrotron X-ray diffraction study, the decomposition of boric acid in IR and Raman experiments starts at lower pressure.²⁰ We attribute this discrepancy to the different rates of the sample compression. While the time interval between successive pressure steps in synchrotron X-ray diffraction measurements was around 15 min, the sample was kept for more than an hour without additional compression of the DAC in IR and Raman studies. We believe that the critical pressure of the decomposition also depends on a compression rate, although no special study was conducted to verify this.

During the decomposition of boric acid, the new bands in the Raman spectra at 194, 576, 880, 905, 1085, 1147 cm^{-1} (see Figure 10 for spectra details) and at 3170, 3277, 3621 cm^{-1} (Figure 8b) progressively substitute the peaks originating from H_3BO_3 . Some of these bands (e.g., 576, 880, and 905 cm^{-1}) likely correspond to vibrations of four-coordinated boron atoms from cubic metaboric acid, HBO_2 . A softening on further compression of the Raman bands observed at 3170 and 3277 cm^{-1} at 1.9 GPa (Figure 8b) is a specific feature of a hydrogen bond in ice.²¹ Consequently, these two peaks can be assigned to the $\nu_1(\text{A}_{1g})$ symmetric stretching and $\nu_3(\text{E}_g)$ antisymmetric stretching of the O–H bonds in ice.²² The peak at 3621 cm^{-1} is likely to correspond to a stretching mode of a non hydrogen bonded monomeric O–H group.²³

In the respective IR spectra during decomposition, the shoulder at 3330–3340 cm^{-1} becomes the main band with the band at 3270 cm^{-1} becoming a shoulder. In the low-frequency region of the IR spectra, the new bands at 640 and 740 cm^{-1}

appear and the initially observed band at 840 cm^{-1} becomes more intense. The former new bands disappear as soon as the active stage of the decomposition process is accomplished and cannot be seen in the IR spectra at 2.2 GPa.

Several alterations in Raman and IR spectra occurred on pressure increase from 2.2 to 3.2 GPa. The most pronounced one was the decrease of the bands intensities, probably associated with the reduction of the scattering volume of the sample. However, the rise of the Raman peak at about 3620 cm^{-1} with increasing pressure indicates that a lower scattering volume is only a partial reason for the Raman and IR intensity drop. The IR active $\nu_2(\text{E}_{1u})$ at 1520 cm^{-1} and $\nu_4(\text{A}_u)$ (in Durig's assignment) at 840 cm^{-1} bands vanish at about 3.2 GPa together with the shoulder at 3270 cm^{-1} . The shape of the band centered near 3400 cm^{-1} at 3.9 GPa is similar to that at zero pressure. This band can be assigned to a poorly resolved doublet of O–H stretching vibrations in ice-VII phase observed in IR studies of ice (see, for example, M. Song et al.²⁴ and references herein). At the same time, the Raman spectra exhibit the abrupt change in the relative intensities of the hydrogen-bonded O–H stretching modes during the pressure increase from 2.2 to 2.7 GPa (Figure 8b). In addition, the peak centered at about 600 cm^{-1} splits at 2.7 GPa (Figure 10). The pressure range of the above alterations in the Raman and IR spectra correlates well with the pressure of the complete ice-VI to ice-VII phase transition and complete decomposition of boric acid observed by X-ray diffraction.

In general, the Raman and IR spectra at 2.7 GPa can be attributed only to the products formed during the chemical decomposition of H_3BO_3 but with one notable difference: no H–O–H deformation band, expected for ice-VI or ice-VII phase at about 1700 cm^{-1} , is observed in the IR spectra. At present, the reason for this inconsistency is not entirely clear. A plausible explanation is that the poor quality of the formed ice crystals and/or strains led to strong broadening of the deformation band. Due to a limited information about the Raman and infrared spectra of $\gamma\text{-HBO}_2$,²⁵ the assignment of the observed Raman and IR bands that replace the peaks of H_3BO_3 cannot be done unambiguously. Special study is required to identify the origin of all new Raman and IR bands observed in Figures 8 and 9 during and after decomposition of H_3BO_3 . Difficulties in a correct assignment may arise from a deviation of the structures of $\gamma\text{-HBO}_2$ and ice from the known, as will be discussed latter. For this reason, a clear distinction between the Raman and IR modes originating from the products of the chemical decomposition of H_3BO_3 might not be easily drawn.

Discussion

Despite the difficulties in obtaining a structural model for compressed H_3BO_3 directly from X-ray diffraction data, the combination of structural information available from X-ray diffraction, Raman, and IR spectroscopy experiments allows one to constrain considerably the pressure-induced structural changes in boric acid. Pressure evolution of the Raman and IR spectra definitively prove the asymmetric type of hydrogen bonds in H_3BO_3 . The bands related to the O–H bond stretching soften on compression analogously to a variety of chemical compounds with O–H \cdots O bonds in which correlations between O–H covalent bond distance and O–H frequency shift are well established.²⁶ Thus, an increase of O–H bond length as the O–O distance decreases with increasing pressure in the corresponding O–H \cdots O hydrogen bond of boric acid can be inferred. From the Raman spectra in Figure 8b, it follows that the O–O distance in the O–H \cdots O hydrogen bond decreases

continuously on compression up to the pressure of the chemical decomposition (about 1.9 GPa).

IR and Raman spectra provide also an important conclusion about the symmetry of $\text{B}(\text{OH})_3$ molecules. It follows that the BO_3 skeletal symmetry of $\text{B}(\text{OH})_3$ molecules does not change or changes insignificantly on compression up to the pressure of decomposition. Neither new bands nor splitting or disappearance of the initial bands related to the BO_3 skeletal vibrations were observed in the Raman and IR spectra of H_3BO_3 up to 1.6 GPa. The absence of a big symmetry perturbation of $\text{B}(\text{OH})_3$ molecules also indicates a preservation of the weak character of the interlayer forces despite a decrease in the interlayer spacing with pressure. The ideal layer separation ($z = 1/4$ and $3/4$) in boric acid decreases from 3.211 Å at ambient pressure to 2.875 Å at 2.2 GPa. The latter distance is still comparatively much greater than the characteristic B–O distances of about 1.36 Å in $\text{B}(\text{OH})_3$ molecules^{2,16} and greater than B–O distances in the tetrahedral units of a metaboric acid (from about 1.45 to 1.5 Å^{27,28}). At ambient pressure, none of the atoms in H_3BO_3 structure is displaced more than 0.11 Å out of the ideal plane position.² Consequently, it is necessary to assume considerable changes in the plane structure on compression to onset strong interlayer interactions by approaching boron and oxygen atoms lying in different planes. Taking into account the above evidences of a symmetry preservation of $\text{B}(\text{OH})_3$ molecules on compression, such changes can proceed only via displacements and rotations of $\text{B}(\text{OH})_3$ complexes as rigid bodies.

Several arguments, however, indicate an essentially unchanged layer structure upon compression. As mentioned above, a significant perturbation of the layer symmetry of H_3BO_3 would be reflected in the Raman and IR spectra, and this is not observed experimentally. In particular, a significant rotation and/or displacement of $\text{B}(\text{OH})_3$ molecules should discriminate the O–O distances in respective O–H \cdots O hydrogen bonds increasing one of them and decreasing others. Such alterations in O–O distances would be manifested by a splitting of O–H stretching vibrations in the Raman spectra with essentially different pressure behavior. The observed two lattice modes around 200 cm^{-1} in the Raman spectra also should be affected by significant changes in the layers structure, however they do not exhibit any singular behavior with increasing pressure.

The latter considerations led us to conclude that the structural changes of H_3BO_3 are mostly associated with the perturbations in a stacking order of sheets. According to the present X-ray diffraction and IR/Raman studies, a new stacking sequence of sheets of $\text{H}(\text{BO})_3$ molecules progressively substitute the 2-layered structure of boric acid starting from about 1 GPa (perhaps, even from lower pressure, e.g., 0.35 GPa). At the same time, the appearance of the shoulder near the $\nu_1(\text{E}_{1u})$ O–H bond stretching vibration in the IR spectra indicates alterations in hydrogen bonding of $\text{H}(\text{BO})_3$ molecules in the structure of boric acid. With decreasing layer separation, the out-of-plane displacements of hydrogen atoms may result in the formation of a hydrogen bond connecting the two nearest oxygen atoms lying in the neighboring layers. The formation of such an interlayer hydrogen bond can be expected, because the shortest interlayer O–O distances (the ideal layer separation is 2.959 Å at 1.1 GPa) become comparable, for example, with the O–O separations in O–H \cdots O hydrogen bonds of ice-VI or ice-VII.^{29,30} Interlayer hydrogen bonds should be metastable with a lifetime depending on the shape of the double-well hydrogen potential along the two oxygen atoms. One can expect that a decrease of the shortest interlayer O–O distances and approximation to the

intralayer O–O distances will increase a lifetime of the interlayer hydrogen bonds and consequently will stabilize a population of hydrogen atoms in new states in a kind of a dynamic equilibrium with a population of hydrogen atoms in the initial O–H \cdots O system. It can also be expected that the concentration of the displaced protons will steadily increase with pressure. Geometrical considerations invoked above do not exclude also the formation of hypervalent B \cdots O bonds resulting in a four coordinated boron atom in a $\text{O}_3\text{B}\cdots\text{O}$ system. The hypervalent bond of the boron atom has been known for many decades. The analysis of a number of oxy-borate structures allowed for establishing the relationship that describes the transformation of planar BO_3 triangle into a pyramidal four-atom system.³¹ For the height h of a pyramid less than 0.1 Å, the relationship $R(\text{Å}) = 2.9 - 10 \cdot h$ is applicable to deduce a distance R between the apex of BO_3 pyramid and the fourth oxygen atom situated on the axis of a pyramid. The distance less than 2.9 Å is consistent with the ideal layer separations in the structure of boric acid at pressures above 1.6 GPa and a planar symmetry of BO_3 complexes (almost zero height for BO_3 pyramid) confirmed by Raman and IR spectroscopy. Consequently, the formation of hypervalent B \cdots O bonds at pressures just below the decomposition pressure range can be expected. The experimental evidence for such bonds can be a slight softening of IR active $\nu_2(\text{E}_{1u})$ and $\nu_4(\text{A}_u)$ (in Durig's assignment) bands. The latter changes would reflect the reduction of the force constants for the three initial B–O covalent bonds at the formation of the fourth B \cdots O bond.^{32,33} Such an interpretation implies that the band observed at 840 cm^{-1} should be assigned to the $\nu_5(\text{A}_u)$ out-of-plane BO_3 angle deformation mode, as was initially proposed by Bethell and Sheppard,¹⁴ rather than to the $\nu_4(\text{A}_u)$ out-of-plane O–H deformation mode. The rise of intensity of this band during chemical decomposition and a strong intensity correlation with $\nu_2(\text{E}_{1u})$ B–O bond stretching mode at higher pressures are consistent with Bethell and Sheppard's assignment. At the same time, the band at 740 cm^{-1} , which appears during chemical decomposition, can be associated with the B–O–H out-of-plane bent.

In terms of the transition state theory for chemical reactions,³⁴ the resulting new local configuration of atoms in a pre-translational structure of boric acid can be considered as a transition state complex or activated complex, and an overall rate of the elementary reaction $\text{H}_3\text{BO}_3 \rightarrow \text{HBO}_2 + \text{H}_2\text{O}$ will be defined by the product of two terms: a number of activated complexes and a frequency with which a complex decomposes to yield the products. The role of pressure in the above chemical reaction is to provide the driving force (a negative free-energy difference between the products HBO_2 and H_2O and the reactant H_3BO_3) as well as to reduce the activation energy (the difference in energy between the activation complex and reactant) of the reaction.

The above scenario of the pressure-induced decomposition of boric acid can be similar to the process of the temperature-induced decomposition, in the sense that increased amplitudes of proton vibrations due to the thermal excitation result in the formation of an activation complex. The fact that either compression or heating of H_3BO_3 gives identical chemical products, that can be attributed to a negative activation volume (more "compact" activation complex) of the reaction $\text{H}_3\text{BO}_3 \rightarrow \text{HBO}_2 + \text{H}_2\text{O}$, resulting in a reaction rate that increases with increasing pressure. Reactions with a negative activation volume generally have negative entropy of activation (the more ordered activation complex) and, consequently, reduced reaction rates.³⁴ Such a relationship between activation volume and entropy

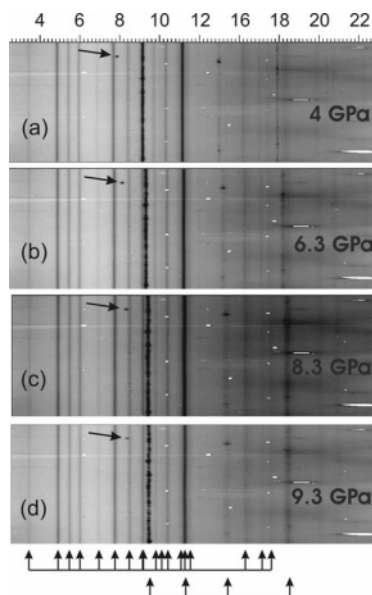


Figure 11. Synchrotron X-ray powder diffraction images obtained during compression of H_3BO_3 after decomposition into HBO_2 and H_2O . Debye–Scherrer diffraction rings were integrated on azimuth as a function of 2θ , resulting in the straight diffraction lines. The pressure-induced shift of the spot indicated by arrows in the images correlates with the shift of the lines originating from ice-VII and indicated by the lower arrows at the bottom of the figure. The “up” arrows indicate the diffraction lines of $\gamma\text{-HBO}_2$.

seems to hold for the transformation of H_3BO_3 into $\text{HBO}_2 + \text{H}_2\text{O}$, which shows a very sluggish kinetics at slow heating.⁶ There is, however, one important peculiarity in the processes of the pressure-induced decomposition of boric acid, which was not recorded in case of slow heating: the formation of a polymorphic modification of H_3BO_3 prior to decomposition. A possible explanation could be that on heating, newly formed water molecules can leave the system, whereas it is impossible in current high-pressure experiment. It is, thus, of interest to perform structural investigation on heating of H_3BO_3 in confined settings, preventing a water loss. We believe that the formation of a new phase of boric acid correlates strongly with the formation of an activation complex. In other words, the activation complex is similar in structure (at least locally) to the new phase of H_3BO_3 . Consequently, a precursor structure of H_3BO_3 can, in some respect, be a characteristic feature of the decomposition process.

It is worthwhile to discuss in conclusion the structural properties of the products, $\gamma\text{-HBO}_2$ and ice-VII, of the chemical decomposition of H_3BO_3 . Close inspection of the pressure–volume data shows a nonlinear behavior of the compressibility of $\gamma\text{-HBO}_2$ phase at low pressures. The extrapolation of the compression curve to the ambient pressure gives a zero-pressure value for the volume essentially higher than one reported in the literature.^{27,28} This result may reflect the fact that during chemical decomposition of boric acid, hydroxyl complexes or entire water molecules are held in the structure of $\gamma\text{-HBO}_2$ and result in an increased volume of metaboric acid. The peak at 3620 cm^{-1} in the Raman spectra of Figure 8b at pressures above 1.9 GPa is attributed to a stretching of OH^- ions, as can be concluded from typical stretching frequency. The small empty cages in the structure of $\gamma\text{-HBO}_2$ ²⁷ perfectly fit the role of traps for these ions. On the other hand, the structure of ice-VII may also be influenced by the $\gamma\text{-HBO}_2$. Evidence of such a possibility is presented in the Figure 11. The sequence of X-ray images shows the presence of crystals with compressibility comparable

to that of ice-VII. The spot observed at 2θ values near 7° cannot be indexed by any known structure of ice. The possible origin of the observed spot can be a new structure of ice with dissolved boron-containing groups formed during decomposition. The formation of this new phase of ice can be similar to the entrapment of carbonate ions by ices.³⁵ Additional studies are required to precisely determine the mechanism and reproducibility of the formation of a potentially new phase of ice.

Conclusions

X-ray diffraction experiments showed that upon compression to ~ 2 GPa, boric acid (H_3BO_3) decomposes into cubic metaboric acid (HBO_2) and ice-VI and ice-VII. The chemical decomposition involves a big overall volume reduction and is preceded by the polymorphic transformation of H_3BO_3 . Complementary Raman and IR spectroscopy measurements are consistent with the results of X-ray diffraction study. The high-pressure Raman and IR spectra suggest that the $\text{B}(\text{OH})_3$ molecular complexes of boric acid mostly preserve their structure up to the pressure of the decomposition (around 1.6 GPa). Formation of interlayer hydrogen bonds and hypervalent $\text{B}\cdots\text{O}$ bonds is proposed as the precursor of the decomposition process. The onset of new hydrogen bonds and formation of $\text{O}_3\text{B}\cdots\text{O}$ groups may be responsible for the pressure-induced phase transition and the reduction of the compressibility of the molecular H_3BO_3 crystal. On the other hand, the presence of a metastable $\text{O}-\text{H}\cdots\text{O}$ configuration results in proton disorder and, possibly, proton mobility in compressed H_3BO_3 .

Acknowledgment. A.A.S. acknowledges support from Alexander von Humboldt Foundation. A.S.P. thanks PRONEX/CNPQ for support.

References and Notes

- (1) Zachariasen, W. H. *Z. Kristallogr.* **1934**, *88*, 150.
- (2) Zachariasen, W. H. *Acta Crystallogr.* **1954**, *7*, 305.
- (3) Zapol, P.; Curtiss, L. A.; Erdemir, A. *J. Chem. Phys.* **2000**, *113*, 3338.
- (4) Erdemir, A.; Bindal, C.; Zuiker, C.; Zavrun, E. *Surf. Coat. Technol.* **1996**, *507*, 86–87.
- (5) Kracek, F. C.; Morey, G. W.; Merwin, H. E. *Am. J. Sci. A* **1938**, *235*, 143.
- (6) Broadhead, P.; Newman, G. A. *J. Mol. Struct.* **1971**, *10*, 157. See also references therein.
- (7) Pereira, A. S.; Perottoni, C. A.; da Jornada, J. A. H. *J. Raman Spectrosc.* **2003**, *34*, 578.
- (8) Pereira, A. S.; Haines, J.; Kuznetsov, A. Yu.; da Jornada, J. A. H. Unpublished.
- (9) Shuvalov, R. R.; Burns, P. C. *Acta Crystallogr., Sect. C: Cryst. Struct. Commun.* **2003**, *59*, i47.
- (10) Mao, H. K.; Bell, P. M.; Shaner, J. W.; Steinberg, D. J. *J. Appl. Phys.* **1978**, *49*, 3276.
- (11) Hammersley, A. P.; Svensson, S. O.; Hanfland, M.; Fitch, A. N.; Hausermann, D. *High Press. Res.* **1996**, *14*, 235.
- (12) Jeanloz, R.; Hazen, R. M. *Am. Mineral.* **1991**, *76*, 1756.
- (13) Birch, F. *J. Geophys. Res.* **1978**, *83*, 1257.
- (14) Bethell, D. E.; Sheppard, N. *Trans. Faraday Soc.* **1955**, *51*, 9.
- (15) Servoss, R. R. *J. Chem. Phys.* **1957**, *26*, 1175.
- (16) Hornig, D. F. *J. Chem. Phys.* **1957**, *26*, 637.
- (17) Durig, J. R. *J. Mol. Struct.* **1968**, *2*, 19.
- (18) Zaki, K.; Pouchan, C. *Chem. Phys. Lett.* **1995**, *236*, 184.
- (19) Schmidt, C.; Thomas, R.; Heinrich, W. *Geochim. Cosmochim. Acta* **2005**, *69*, 275.
- (20) In the angle-dispersive X-ray study performed in laboratory conditions, during which the sample was kept at a given pressure for at least 48 h, we already had evidences of the decomposition at 1.4 GPa. During the first study by EDXRD, the pressure, after the disappearing of the diffraction peaks, decreased from 2 to 1.7 GPa.
- (21) Walrafen, G. E.; Abebe, M. *J. Chem. Phys.* **1982**, *77*, 2166.
- (22) Pruzan, P.; Chervin, J. C.; Gauthier, M. *Europhys. Lett.* **1990**, *13*, 81.

- (23) Mayo, D. W.; Miller, F. A.; Hannah, R. W. *Course Notes on the Interpretation of Infrared and Raman Spectra*; John Wiley and Sons: New Jersey, 2004; Chapter 6, p 163.
- (24) Song, M.; Yamawaki, H.; Fujihisa, H.; Sakashita, M.; Aoki, K. *Phys. Rev B: Condens. Matter Mater. Phys.* **1999**, *60*, 12644.; Song, M.; Yamawaki, H.; Fujihisa, H.; Sakashita, M.; Aoki, K. *Phys. Rev B: Condens. Matter Mater. Phys.* **2003**, *68*, 24108.
- (25) Bertoluzza, A.; Monti, P.; Battaglia, M. A.; Bonora, S. *J. Mol. Struct.* **1980**, *64*, 123.
- (26) Olovsson, I.; Jönsson, P. G. In *The Hydrogen Bond 2: Structure and Spectroscopy*; Schuster, P., Zundel, G., Sandorfy, C., Eds.; North-Holland Pub. Co.: Amsterdam, 1976; Vol. 1, p 393.
- (27) Freyhardt, C. C.; Wiebcke, M.; Felsche, J. *Acta Crystallogr., Sect. C: Cryst. Struct. Commun.* **2000**, *56*, 276.
- (28) Zachariasen, W. H. *Acta Crystallogr.* **1963**, *16*, 380.
- (29) Kamb, B. *Science* **1965**, *150*, 205.
- (30) Nemes, R. J.; Loveday, J. S.; Marshall, W. G.; Hamel, G.; Besson, J. M.; Klotz, S. *Phys. Rev. Lett.* **1998**, *81*, 2719.
- (31) Zobetz, E. Z. *Kristallogr.* **1982**, *160*, 81.
- (32) Badger, R. M.; Bauer, S. H. *J. Chem. Phys.* **1937**, *5*, 839.
- (33) Yukhnovich, G. V.; Kargov, S. I.; Merzlyak, T. T. *Izv. RAS, Chem. (English Translation Russ. Chem. Bull.)* **1999**, *12*, 2237.
- (34) Lasaga, A. C. *Kinetic Theory in the Earth Sciences*; Princeton University Press: Princeton, 1998; Chapter 2, p 152.
- (35) Martinez, I.; Sanchez-Valle, C.; Daniel, I.; Reynard, B. *Chem. Geol.* **2004**, *207*, 47.